NEOPLASIA
www.neoplasia.com

Volume 12 Number 10 October 2010 pp. 778–788 778

An Anti–Urokinase Plasminogen Activator Receptor Antibody (ATN-658) Blocks Prostate Cancer Invasion, Migration, Growth, and Experimental Skeletal Metastasis *In Vitro* and *In Vivo*[1]

Shafaat A. Rabbani*, Bushra Ateeq*, Ani Arakelian*, Maria Luisa Valentino*, David E. Shaw[†,‡], Lisa M. Dauffenbach[§], Christopher A. Kerfoot[§] and Andrew P. Mazar[¶,2]

*Department of Medicine, McGill University, Montreal, Quebec, Canada; [†]D.E. Shaw Research, New York, NY, USA; [‡]Center for Computational Biology and Bioinformatics, Columbia University, New York, NY, USA; [§]Mosaic Laboratories, LLC, Lake Forest, CA, USA; [¶]Attenuon LLC, San Diego, CA, USA

Abstract

Urokinase plasminogen activator receptor (uPAR) is a multidomain protein that plays important roles in the growth, invasion, and metastasis of a number of cancers. In the present study, we examined the effects of administration of a monoclonal anti-uPAR antibody (ATN-658) on prostate cancer progression *in vitro* and *in vivo*. We examined the effect of treatment of ATN-658 on human prostate cancer cell invasion, migration, proliferation, and regulation of intracellular signaling pathways. For *in vivo* studies, PC-3 cells (1×10^6) were inoculated into the right flank of male Balb C *nu/nu* mice through subcutaneous or through intratibial route (2×10^5) of male Fox Chase severe combined immunodeficient mice to monitor the effect on tumor growth and skeletal metastasis. Treatment with ATN-658 resulted in a significant dose-dependent decrease in PC-3 cell invasion and migration without affecting cell doubling time. Western blot analysis showed that ATN-658 treatment decreased the phosphorylation of serine/threonine protein kinase B (AKT), mitogen-activated protein kinase (MAPK), and focal adhesion kinase (FAK) without affecting AKT, MAPK, and FAK total protein expression. In *in vivo* studies, ATN-658 caused a significant decrease in tumor volume and a marked reduction in skeletal lesions as determined by Faxitron x-ray and micro–computed tomography. Immunohistochemical analysis of subcutaneous and tibial tumors showed a marked decrease in the levels of expression of pAKT, pMAPK, and pFAK, consistent with the *in vitro* observations. Results from these studies provide compelling evidence for the continued development of ATN-658 as a potential therapeutic agent for the treatment of prostate and other cancers expressing uPAR.

Neoplasia (2010) 12, 778–788

Introduction

Overexpression of the urokinase plasminogen activator receptor (uPAR) has been demonstrated in several different cell types found in tumors, including the tumor cells themselves, angiogenic endothelial cells, and tumor-infiltrating inflammatory cells but rarely in normal tissue [1–3]. uPAR expression has been detected in numerous solid tumor types, including prostate cancer, where uPAR expression has been demonstrated to be associated with high-risk disease and to have a prognostic role [4,5]. uPAR is involved in numerous activities associated with tumor progression, including tumor cell proliferation and survival, migration and invasion, angiogenesis, and metastasis [6–9] and, as such, represents a well-validated therapeutic target for the treatment of cancer. However, despite copious amounts of data supporting the therapeutic targeting of this receptor, there are currently no uPAR-targeted therapeutics in human clinical trials.

Address all correspondence to: Dr Shafaat A. Rabbani, McGill University Health Centre, 687 Pine Avenue West, Room H4.67, Montreal, Quebec, Canada H3A 1A1.
E-mail: shafaat.rabbani@mcgill.ca

[1]This work was supported by a grant from the Canadian Institutes for Health Research MOP 12609.

[2]Present address: Chemistry of Life Processes Institute and Robert H. Lurie Cancer Center, Northwestern University, Evanston, IL 60208. E-mail: a-mazar@northwestern.edu.

Received 18 February 2010; Revised 15 June 2010; Accepted 15 June 2010

DOI 10.1593/neo.10296

Historically, attempts at targeting uPAR have focused on attenuating cell surface proteolysis by inhibiting the binding of the zymogen form of urokinase plasminogen activator (single-chain uPA [scuPA]), long considered the main ligand for uPAR, to the cell surface, which decreases the catalytic efficiency of scuPA activation by several hundred fold [10]. These approaches have experienced a number of problems and, when tested in animal tumor models, have exhibited modest activity at best [11,12], leading to the current paucity of therapeutic agents targeting uPAR in the clinic.

Effects of uPAR are mediated through the activation of key intracellular signaling pathways. A number of extracellular epitopes that interact with these signaling mediators are located within domains 2 and 3 (D2 and D3) of uPAR. In recent years, it has become apparent that uPAR has multiple ligands in addition to uPA. Many of these ligands (integrins, extracellular matrix components, and growth factor receptors) have independently been identified as being important to tumor progression [13–15], suggesting that targeting some of these other interactions of uPAR may also have therapeutic utility. In addition, genetic knockdown approaches in several studies demonstrated that decreasing uPAR expression had profound effects on tumor growth, in contrast to what had been observed with approaches targeting uPA binding [16,17]. These results led to the hypothesis that interfering with the interaction of uPAR with one or more of its other, non-uPA ligands might lead to a more robust antitumor effect. To address this hypothesis, a uPAR fragment-based immunization approach was used to generate a panel of anti-uPAR monoclonal antibodies with the idea of identifying clones that did not block the binding of uPA to uPAR but would bind to other epitopes on uPAR that might be important to some of the other biologic functions of this receptor. One such antibody, ATN-658, a mouse IgG1, is able to bind to D2D3 of uPAR with high affinity (K_d ~ 1 nM), does not inhibit the binding of uPA to uPAR, and is able to bind to uPAR even when uPA was also bound. ATN-658 inhibits invasion, migration, and, in some cell types, proliferation [18]. Thus, ATN-658 may exemplify a new paradigm for the targeting of uPAR.

Because of the association of uPAR with high-risk disease and prognosis in patients with prostate cancer, ATN-658 was evaluated in this study for its ability to inhibit the growth of both primary and metastatic prostate cancer tumors using the PC-3 human prostate adenocarcinoma cell line.

Materials and Methods

Cell Culture and Treatment

Human prostate cancer cell line PC-3 and the cervical carcinoma cell line HeLa were obtained from the American Type Culture Collection (Manassas, VA). Cells were maintained in RPMI 1640 medium (Invitrogen Life Technologies, Burlington, Ontario, Canada) with 2 mM L-glutamine, 10% FBS, and 100 U/ml of penicillin-streptomycin sulfate. Cells were incubated at 37°C in 5% CO_2.

Antibodies

The anti–mitogen-activated protein kinase (MAPK) antibody (ERK1, catalog no. SC-94, rabbit IgG) was purchased from Santa Cruz Biotechnologies (Santa Cruz, CA). The anti–phosphorylated MAPK antibody (clone 20G11, catalog no. 4376, rabbit IgG) and anti–phosphorylated serine/threonine protein kinase B (AKT) antibody (pAKT, catalog no. 3787, rabbit IgG) were purchased from Cell Signaling (Danvers, MA); anti-AKT antibody (catalog no. Ab8805, rabbit IgG) was purchased from Abcam (Cambridge, MA); anti–phosphorylated FAK antibody (pFAK, catalog no. 44-624G, rabbit IgG) was purchased from Biosource (Camarillo, CA); anti–focal adhesion kinase (FAK) antibody (catalog no. 1700-1, rabbit IgG) was purchased from Epitomics (Burlingame, CA). The mouse and rabbit IgG isotype control antibodies were purchased from Dako (Carpinteria, CA). These antibodies were validated at Mosaic Laboratories (Lake Forest, CA) for use in detecting their respective antigens and were used as described in Immunohistochemical Analyses. ATN-658, which does not block the binding of uPA to uPAR, and ATN-617, which does block binding of uPA to uPAR, were raised against D2D3 of uPAR as previously described [18].

Cell Binding Assays

scuPA was radiolabeled using iodine I 125 (^{125}I), and competition binding assays were carried out as previously described [19]. The binding and wash buffer for the binding assays was Hank's balanced salt solution 0.1% BSA. Briefly, HeLa cells were seeded into 24-well plates (150,000 cells per well) and allowed to adhere for 24 hours before use. For the competition studies, medium was aspirated, and 500 μl of either ATN-617 or ATN-658 at different concentrations was added to the wells followed by ^{125}I-scuPA (0.2 nM; 20,000 cpm/well). The plates were incubated for 1 hour at room temperature followed by aspiration of the binding buffer and washing of the cells (3× with 0.5 ml of wash buffer). The cells were then lysed, the lysates were transferred to tubes, and the amount of ^{125}I-scuPA in each well was measured using a gamma counter.

The direct binding of ATN-658 was measured as follows. ATN-658 was biotinylated using a commercially available kit (EZ-link sulfo-NHS-LC-biotin; Pierce Chemical, Rockford, IL) as per the manufacturer's instructions. Biotin–ATN-658 bound with similar affinity to nonbiotinylated ATN-658 was measured in a competition study using HeLa cells (data not shown). PC-3 cells (50,000 cells per well in 96-well plates) were plated and allowed to adhere overnight in culture medium with 10% FBS. Biotin-ATN-658 was diluted in PBS with 0.1% casein at different concentrations of antibody. Cells were washed (3×) with PBS with 0.05% Tween-20, and different concentrations of biotin–ATN-658 were added and incubated for 1 hour at 37°C. Cells were washed again (5×) using PBS with 0.05% Tween-20 and OPD substrate (200 μl per well) was added and incubated for 15 minutes at room temperature in the dark. The reaction was quenched using 1 M H_2SO_4, and the color developed was read at 490 nm using an absorbance plate reader.

Cell Proliferation Assay

Prostate cancer cells (PC-3 and DU-145) were plated in duplicate at a density of 50,000 cells per well in 2 ml of culture medium in six-well plates. Cells were grown in regular medium with 10% FBS in control and treatment (ATN-658) group. Cell growth was analyzed at two different doses of ATN-658 (10 and 50 μg/ml). Cells were trypsinized, and the number of viable cells was determined using 0.4% trypan blue and counted at different time points starting from day 1 using a Coulter counter (model ZF; Coulter Electronics, Harpenden, Hertfordshire, UK). Cell culture medium was replenished every second day along with the indicated dose of ATN-658 in the treatment group. The experiment was repeated twice.

Boyden Chamber Matrigel Invasion Assay

PC-3 and DU-145 cell invasive capacity was determined using a two-compartment Boyden chamber Matrigel invasion assay (Transwell; Costar Corning Corporation, Lowell, MA) as described previously

[20]. The 8-μm pore polycarbonate filters were coated with Matrigel (50 μg/filter). Medium containing 5×10^4 cells and ATN-658 (10 and 50 μg/ml) or control IgG was resuspended in 0.1 ml of serum-free medium and added to the upper chamber. This was then placed on top of the lower chamber that was prefilled with 0.8 ml of serum-free medium supplemented with 25 μg/ml fibronectin (Sigma Aldrich, Oakville, Ontario, Canada). The cells were allowed to invade through the Matrigel (BD Biosciences, Mississauga, Ontario, Canada) onto the filters for 18 hours at 37°C. After incubation, the medium was removed, and the polycarbonate filters with invaded cells were fixed in 2% paraformaldehyde, 0.5% glutaraldehyde (Sigma Aldrich) in 0.1 M phosphate buffer pH 7.4, at room temperature for 30 minutes. The filters were washed twice with PBS, stained for 5 minutes with 0.5% toluidine blue, and washed again with PBS and mounted onto glass slides. The number of cells invaded was examined under a light microscope at a magnification of 40×. Ten random fields from each experimental group were counted and the number of cells invaded was calculated. The experiment was repeated three times.

Cell Migration Assay

Prostate cancer cells (PC-3 and DU-145) were grown in six-well plates in RPMI + 10% FBS. Once the cells were 100% confluent, the cell monolayer was mechanically scratched in the center of each well with a sterile 1000-μl pipette tip. The medium and nonadherent cells were aspirated, and the cells were washed with serum-free media. Control cells were grown in RPMI + 2% FBS, and treated cells were grown in RPMI + 2% FBS containing 10 and 50 μg/ml of ATN-658 for 24 hours where the culture medium was changed at 6 hours. Cells were then washed three times with serum-free medium to get rid of the nonadherent cells and debris. Cell migration was monitored at different time points with an inverted bright field microscopy under the 4× objective. Only cell-free area was selected, measured, and quantified using Image ProPlus software and calculated as percentage cell migration using the equation: % cell migration = [1 − (scratch area at $T_{x\ (\text{hours})}$/scratch area at T_0], where the T_x is the respective time point and T_0 is the time immediately after the scratch. These experiments were repeated twice.

Western Blot Analysis

Prostate cancer cells (PC-3) were plated in 100-mm petri dishes (1×10^6) and then serum-starved overnight. The following day, the cells were treated with two doses of ATN-658 (10 and 50 μg/ml) in the presence of 2% FBS for 24 hours. The cells were lysed with complete radioimmunoprecipitation assay buffer, and the protein concentration was determined. The cell lysates was electrophoresed on an SDS–polyacrylamide gel, transferred onto a polyvinylidene difluoride membrane (Bio-Rad Laboratories, Mississauga, Ontario, Canada) and detected using enhanced chemiluminescence detection reagents (Perkin-Elmer Life Sciences, Inc, Boston, MA).

In Vivo Tumor Growth in Prostate Cancer Model

Six-week-old male Balb C *nu/nu* mice were obtained from NCI Research Resources, Frederick, MD. Before inoculation, PC-3 cells growing in serum-containing medium were washed with Hank's balanced buffer, trypsinized, and centrifuged at 1500 rpm for 5 minutes. Cell pellets (2.0×10^6) were resuspended in 200 μl of saline with 20% Matrigel. An anesthetic cocktail of ketamine (50 mg/kg), xylazine (5 mg/kg), and acepromazine (1 mg/kg) was injected intramuscularly, and 2.0×10^6 cells were inoculated using a 26-gauge needle subcutaneously (s.c.) into the right flank of anesthetized mice. Animals were divided into a control group, where animals were treated with mouse IgG1 (intraperitoneally [i.p.] 10 mg/kg, twice a week), and an experimental group, where animals were treated with ATN-658 (i.p. 10 mg/kg, twice a week). This dose of ATN-658 resulted in steady-state plasma levels of 0.5 to 1 μM and exceeded the K_d of ATN-658 for uPAR by 500 to 10,000×.

Both control and experimental animals were monitored at weekly intervals for 7 weeks for tumor development and growth. Tumor volume was determined according to the formula: tumor volume = shorter diameter^2 × longer diameter / 2. Results were presented as the mean of tumor volumes recorded from all animals within a particular cohort. At the end of the study, animals were killed, and primary tumors were removed. Half of the tumors were fixed in 10% buffered formalin for immunohistochemical analysis, and the other half were snap-frozen in liquid nitrogen.

In studies designed to evaluate the effect of ATN-658 on the outgrowth of PC-3 "metastases" in the bone, six-week-old male Fox Chase severe combined immunodeficient (SCID) mice were obtained from Charles River (St Constant, Quebec, Canada). Before inoculation, PC-3 cell pellets (2×10^5 cells) were resuspended in 40 μl of saline and injected with a 26-gauge needle into the tibia using a drilling motion. Animals were randomized into a control group, where animals were treated with mouse IgG (i.p. 10 mg/kg, twice a week), and an experimental group, where animals were treated with ATN-658 (i.p. 10 mg/kg, twice a week). Mice were monitored weekly for tumor burden. On week 4, digital radiography of hind limbs was done using a Faxitron x-ray machine (Faxitron X-ray Corp, Wheeling, IL) to monitor the development of skeletal lesions. At week 5, mice were killed, and the left tibia was collected, decalcified, and fixed in formalin for further immunohistochemical analysis. Skeletal lesions were calculated as described by Yang et al. [21], where 0 = no lesions, 1 = minor lesions, 2 = small lesions, 3 = significant lesions with minor break of margins, or 4 = significant lesions with major break in peripheral lesions. Radiologically affected tibia were fixed, decalcified, paraffin-embedded, and subjected to histologic analysis as previously described [22]. In all *in vivo* studies, eight animals were used in each group, radiologic evidence of tumor is seen at week 3, and treatment with ATN-658 was started 1 day after tumor cell inoculation. All the experimental animal protocols were in accordance with the McGill University Animal Care Committee guidelines.

Immunohistochemical Analyses

Formalin-fixed, paraffin-embedded tissue blocks containing PC-3–derived tumor tissues were sectioned at 4 μm and mounted onto positively charged glass slides for immunostaining. Sections were baked at 60°C for 20 minutes, deparaffinized through three changes of xylene, and rehydrated through graded alcohols. After rehydration, tissue sections were incubated in 3% hydrogen peroxide for 5 minutes to quench endogenous peroxidase, followed by antigen retrieval as indicated in Table 1. Slides were rinsed in Splash-T Buffer (Mosaic Laboratories) for 5 minutes and incubated with primary antibodies diluted in Dako Antibody Diluent (Dako) for the time indicated in Table 1. Slides were washed in three changes of Splash-T buffer for 5 minutes, and detection was performed using the Envision+ detection kit (Dako). Slides were washed in three changes of Splash-T buffer for 5 minutes, and color was developed using DAB (Dako) for 5 minutes. Slides were washed in distilled water, counterstained with hematoxylin, dehydrated

Table 1. Summary of Immunohistochemistry Methods.

Antibody	Source	Antigen Retrieval	Dilution	Incubation Time (min)
Ki-67	Thermo Scientific	HighTide 40 min at 95°C	1:800	30
Murine CD31	Santa Cruz Biotechnologies	BORG 3 min at 125°C	1:1600	30
uPAR	Attenuon	DIVA 30 sec at 125°C	1:10,000	30
CC3	Cell Signaling	HighTide 40 min at 95°C	1:320	30
Akt	Abcam	DIVA 40 min at 95°C	1:2000	120
pAkt (S473)	Cell Signaling	HighTide 40 min at 95°C	1:40	120
ERK	Santa Cruz Biotechnologies	DIVA 30 sec at 125°C	1:6400	30
pERK (T202 and Y204)	Cell Signaling	DIVA 3 min at 125°C	1:100	30
FAK	Epitomics	DIVA 3 min at 125°C	1:240	overnight
pFAK (Y397)	Biosource	Proteinase K	1:400	30

through graded alcohols, cleared through three changes of xylene, and coverslipped.

The staining intensity for each antibody was judged relative to the intensity of a control slide containing an adjacent section stained with an irrelevant, negative control antibody that is species- and isotype-matched to the test article. Staining of the section labeled with the negative reagent control is considered "background." A score of 0 indicates no staining relative to background, 1+ indicates weak staining, 2+ indicates moderate staining, and 3+ indicates strong staining. Total positive staining (the sum of all staining at 1+, 2+, and 3+) was recorded for each specimen.

Statistical Analysis

Results were analyzed as the mean ± SE, and comparisons of the experimental data were analyzed by an independent two-sample t' test at the $P < .05$ level of significance.

Results

Effect of ATN-658 on Cell Proliferation Invasion and Migration

The ability of ATN-658 to compete ^{125}I-scuPA binding to HeLa cells, which express uPAR but not uPA, is shown in Figure 1*A*. ATN-617 is a control antibody that is known to inhibit the binding of uPA to uPAR. In another set of studies, the binding of biotinylated ATN-658 directly to PC-3 cells was measured. Biotin–ATN-658 bound to these cells in a saturable manner with a K_d ~ 1 nM, similar to the K_d observed for ATN-658 binding to HeLa in the absence of scuPA (Figure 1*B*).

The levels of expression of uPAR and its ligand uPA were examined in human prostate cancer cells. Whereas uPA expression was undetectable in LNCaP cells, it was readily detected in both DU-145 and PC-3 cells (data not shown). The level of uPAR in PC-3 was higher than DU-145 cells and was similar to that seen in HT1080 cells, a fibrosarcoma cell line described to express high levels of uPAR [23]. To evaluate the effect of ATN-658 on prostate cancer cell doubling time, PC-3 and DU-145 cells were treated with different doses of control IgG or ATN-658 for 5 days. Treatment with ATN-658 had no statistically significant effect on prostate cancer cell proliferation (Figure 1*C*).

We then examined the effect of ATN-658 on PC-3 and DU-145 cells' invasive capacity using a Matrigel Boyden chamber invasion assay. Cells treated with ATN-658 exhibited a dose-dependent inhibition in tumor cell invasive capacity compared with cells treated with similar dose of control IgG (Figure 1*D*). These effects were not due to any change in cell proliferation during the incubation period, where ATN-658 had no significant effect as shown in Figure 1*C*.

A cell migration assay was also performed. PC-3 and DU-145 cells were treated with different doses of control IgG or ATN-658 for 24 hours. After the end of this treatment period, cells were allowed to migrate for different periods (3, 6, and 24 hours). The highest dose (50 μg/ml) of ATN-658 tested had a statistically significant effect on reducing cell migration in both the uPAR expressing prostate cancer cell lines (PC-3 and DU-145) after 24 hours (Figure 1, *E* and *F*), whereas no effect was observed on non–uPAR-expressing LNCaP cells (data not shown). Throughout the course of these studies, no significant effect on PC-3 cell morphology was observed after treating with ATN-658 at any of the doses tested. Control IgG or a uPAR targeted antibody (ATN-617) that inhibited uPA binding to uPAR had no effect on prostate cancer cell invasion and migration (data not shown).

Effect of ATN-658 on Intracellular Signaling Pathways In Vitro

The interaction between uPAR and integrins results in the activation of various intracellular signaling pathways that are known to play important roles in tumor progression. To evaluate the ability of ATN-658 to affect these signaling pathways, PC-3 cells were treated with 50 μg/ml of control IgG or ATN-658 for 24 hours. At the end of this incubation period, cell lysates were subjected to Western blot analysis. Significant inhibition of phosphorylation of AKT, MAPK, and FAK was seen in cells treated with ATN-658 (Figure 2), indicating that this antibody had pleiotropic effects on pathways associated with uPAR-dependent signaling.

Effect of ATN-658 on PC-3 Tumor Growth In Vivo

To test the effect of ATN-658 on tumor growth, PC-3 cells were inoculated s.c. into the right flank of male Balb C *nu/nu* mice. Animals were treated with 10 mg/kg of control IgG or ATN-658 twice weekly through the i.p. route. Tumor volumes were determined at weekly intervals and compared with tumor-bearing animals receiving control, isotype-matched IgG. Experimental animals treated with ATN-658 showed a significant decrease in their tumor volume compared with the control group of animals, which showed a progressive increase in tumor growth throughout the course of these studies (Figure 3).

Effect of ATN-658 on PC-3 Experimental Skeletal Metastasis In Vivo

uPAR/integrin interactions result in the activation of signaling pathways that are involved in skeletal biology and in the development and

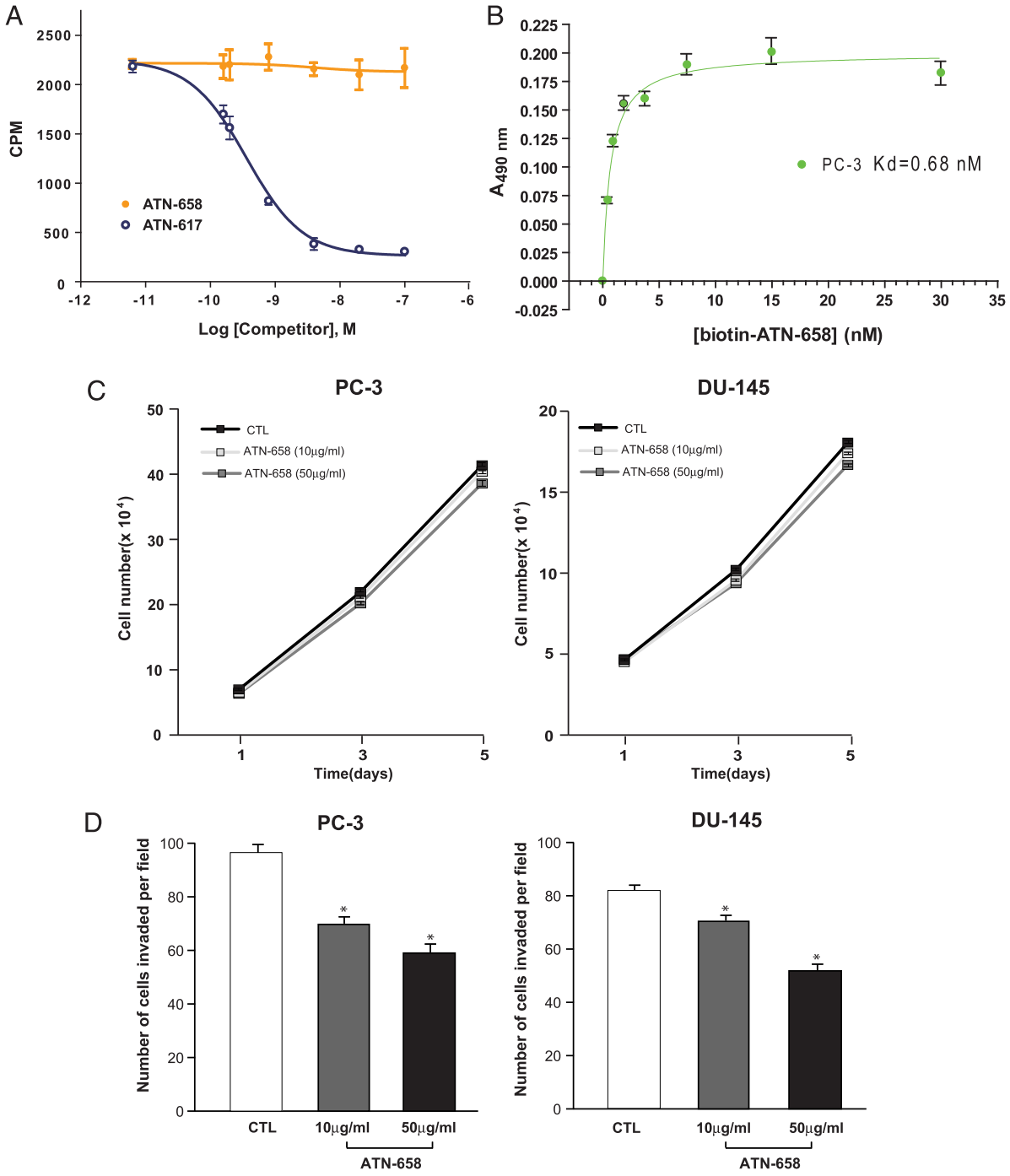

Figure 1. Displacement of uPA binding by ATN-658 to PC-3 and HeLa cells and effect on prostate cancer cell proliferation, invasion, and migration *in vitro*. Binding to HeLa (A) and PC-3 (B) cells was carried out in triplicate at each concentration of antibody as described in Materials and Methods. Human prostate cancer cells PC-3 (left) and DU-145 (right) were plated in six-well plates and treated with control IgG (CTL) or two different doses of ATN-658. Cell growth rate was determined in each group was determined after trypsinization and counting the number of cells as described in Materials and Methods (C). Results are represented as mean ± SEM of duplicate wells for each time point. Similar results were obtained in two independent experiments. PC-3 (left) and DU-145 (right) cell invasive capacity was evaluated after treating with control IgG or ATN-658 using a Boyden chamber Matrigel invasion assay. Number of cells invading is shown as bar diagram ± SEM (D) as described in Materials and Methods. A migration assay was carried out on PC-3 (E) and DU-145 (F) cells in the presence of control IgG or two different doses of ATN-658 in cells culture medium containing 2% FBS as shown in panels E and F. For these studies, cells were seeded at the same density, allowed to grow as monolayer, and scratched as described in Materials and Methods. Migration at different time points was recorded, and percent migration compared with T_0 was calculated. Results are presented as the mean ± SEM of two different experiments (lower panels of E and F). A significant difference from the control (CTL) is represented by an asterisk ($P < .05$).

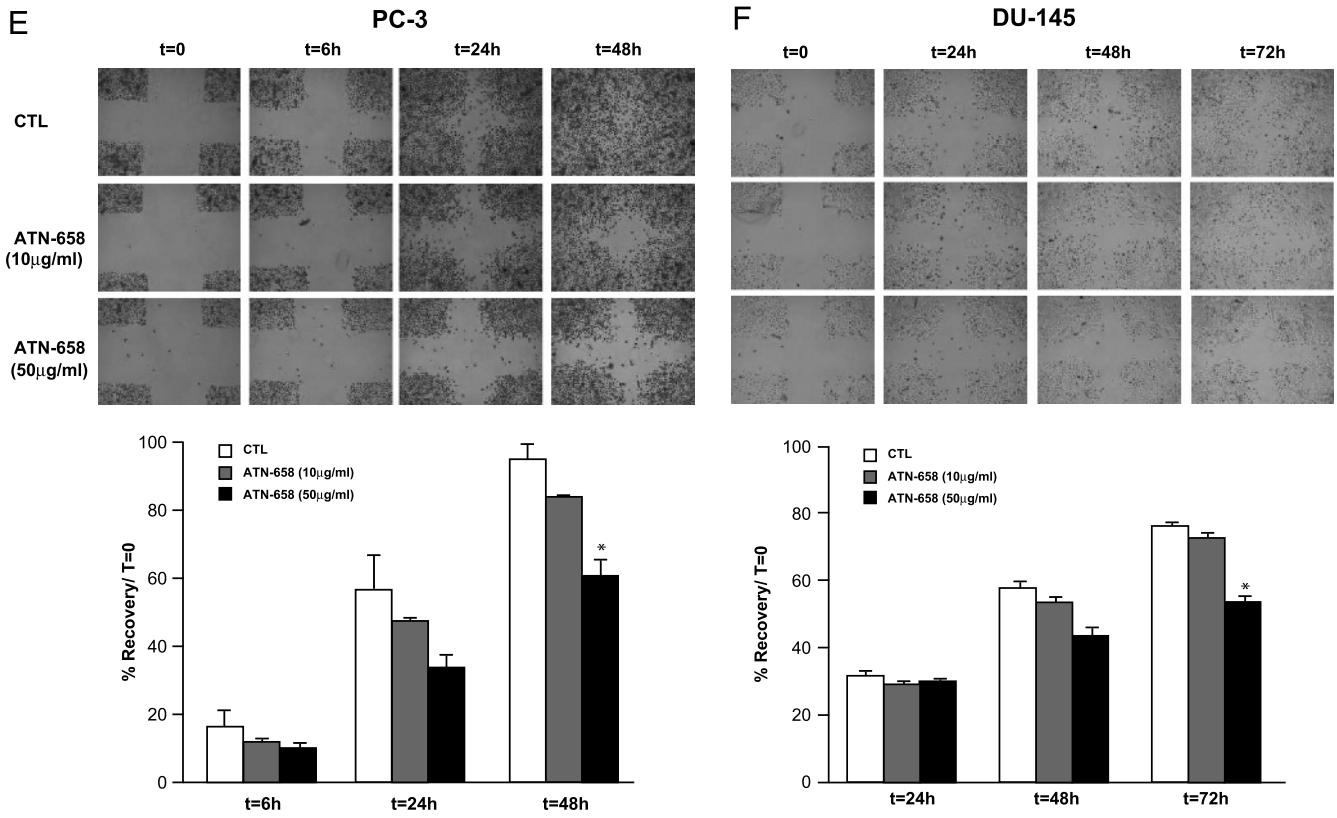

Figure 1. (*continued*).

progression of skeletal metastasis, a common complication in prostate cancer patients. We therefore carried out studies to examine the effect of ATN-658 on PC-3 cell experimental skeletal metastasis. For these studies, PC-3 cells were inoculated directly into the tibia of male Fox Chase SCID mice. Animals were treated with 10 mg/kg control IgG or ATN-658 twice weekly through the i.p. route. Radiologic examination of tibias by was carried out at weekly intervals by Faxitron. A marked decrease in the number and area of skeletal lesions was consistently observed in animals receiving ATN-658 compared with control animals (Figure 4). Although ATN-658 was effective at both weeks 4 (45%) and 5 (65%) after tumor cell inoculation, these effects were more pronounced when treatment was administered for 5 weeks. These antimetastatic effects of ATN-658 were also confirmed by histologic examination of tibia from control and experimental animals (Figure 4).

Effect of ATN-658 on Intracellular Signaling Pathways, Tumor Cell Proliferation, and Gene Expression in Primary Tumors and Experimental Skeletal Metastasis In Vivo

At the end of each *in vivo* study, all control and experimental animals were killed, and tumor-bearing tissue was removed. Primary tumor and tibia were fixed, decalcified (tibia), and subjected to immunohistochemical analysis. The levels of expression of pMAPK and pFAK in both control and ATN-658–treated tumors grown s.c. were similar. However, after treating with ATN-658, a significant reduction in the expression of pAKT was observed in ATN-658–treated s.c. tumors (data not shown). In contrast to tumors grown s.c., a marked reduction in pMAPK, pFAK, and pAKT was seen in the tumors grown in the tibia of animals treated with ATN-658 compared with tibias from mice receiving control IgG (Figure 5). No significant change in the levels of expression of total MAPK, FAK, and AKT was observed between control and experimental s.c. and intratibial (i.t.) tumors (data not shown). Tibia from control and experimental animals were also subjected to immunohistochemical analysis to determine the effect on tumor cell proliferation, angiogenesis, apoptosis, and uPAR expression using antibodies targeting Ki67, cleaved caspase 3 (CC3), CD31, and uPAR. Results from these studies showed no significant change in the levels of expression of CD31 and CC3 after treating with ATN-658 (data not shown). In contrast, treatment with ATN-658 resulted in a significant decrease in KI67 and uPAR expression compared with animals receiving control IgG (Figure 6).

Discussion

The therapeutic targeting of uPAR has proven to be a difficult challenge, and there are currently no uPAR-targeted therapeutic agents being evaluated in human clinical trials. Although the system contains several well-validated targets, only a single molecule, an enzyme inhibitor of uPA, has reached human clinical trials. Thus, the promise of targeting this receptor therapeutically has not been realized and remains to be explored. Studies published in the literature in recent years have elucidated numerous activities for uPAR in addition to tethering uPA to the cell surface. The identification of a number of ligands that bind to uPAR in addition to uPA has opened up the possibility that there might exist other ways of targeting uPAR therapeutically that do not involve inhibiting its interaction with uPA. In fact, being able to target uPAR therapeutically while uPA is bound to uPAR is attractive from a pharmacological standpoint since very often, a large percentage of uPAR is already bound with endogenous uPA and agents that are intended to displace uPA would have a higher barrier to overcome than those that

could bind to uPAR regardless of the presence of uPA. With this in mind, a mouse monoclonal antibody (ATN-658) was identified from a larger panel of monoclonal antibodies raised against proteolytic fragments of uPAR, which did not block the binding of uPA to uPAR and could bind to uPAR even when uPA was also bound. uPA itself can activate several signaling pathways through binding to uPAR, but uPAR-mediated signaling in the absence of uPA is not well understood [24].

In this study, we demonstrate that this antibody inhibits the activation of FAK, AKT, and MAPK in PC-3 cells *in vitro*, signaling pathways that have previously been shown to be activated in a uPAR-dependent manner [13,25]. Although we have not yet identified exactly which interaction of uPAR is inhibited by ATN-658, we do know that this antibody binds to domain 3 of uPAR, and studies are underway to understand how ATN-658 is functioning at the molecular level. In PC-3 cells, the functional result of inhibiting FAK, AKT, and MAPK activation *in vitro* is the inhibition of migration and invasion. We demonstrate that although this inhibition can be observed in uPAR-expressing prostate cancer cell lines (PC-3 and DU-145), these effects are more pronounced in cells (PC-3) expressing high levels of uPAR. For our *in vivo* studies, we focused on evaluating the effect of ATN-658 on PC-3 cell growth in models of s.c. and i.t. growth. PC-3 cells express high levels of uPAR, comparable to the HT1080 cell line, a well-characterized uPAR-expressing fibrosarcoma line [22]. PC-3 cells are the best characterized and most frequently used prostate line in the i.t. model, another reason for using this cell line *in vivo*. In experienced hands, the rate of tumor take in these models can be 100%, which allows full evaluation of the efficacy of potential therapeutic agents as shown in the current study. It should be noted that, in models of pancreatic [18] and colon cancer [25], inhibition of proliferation by ATN-658 has also been observed albeit only *in vivo*. In the current PC-3 study, ATN-658 also

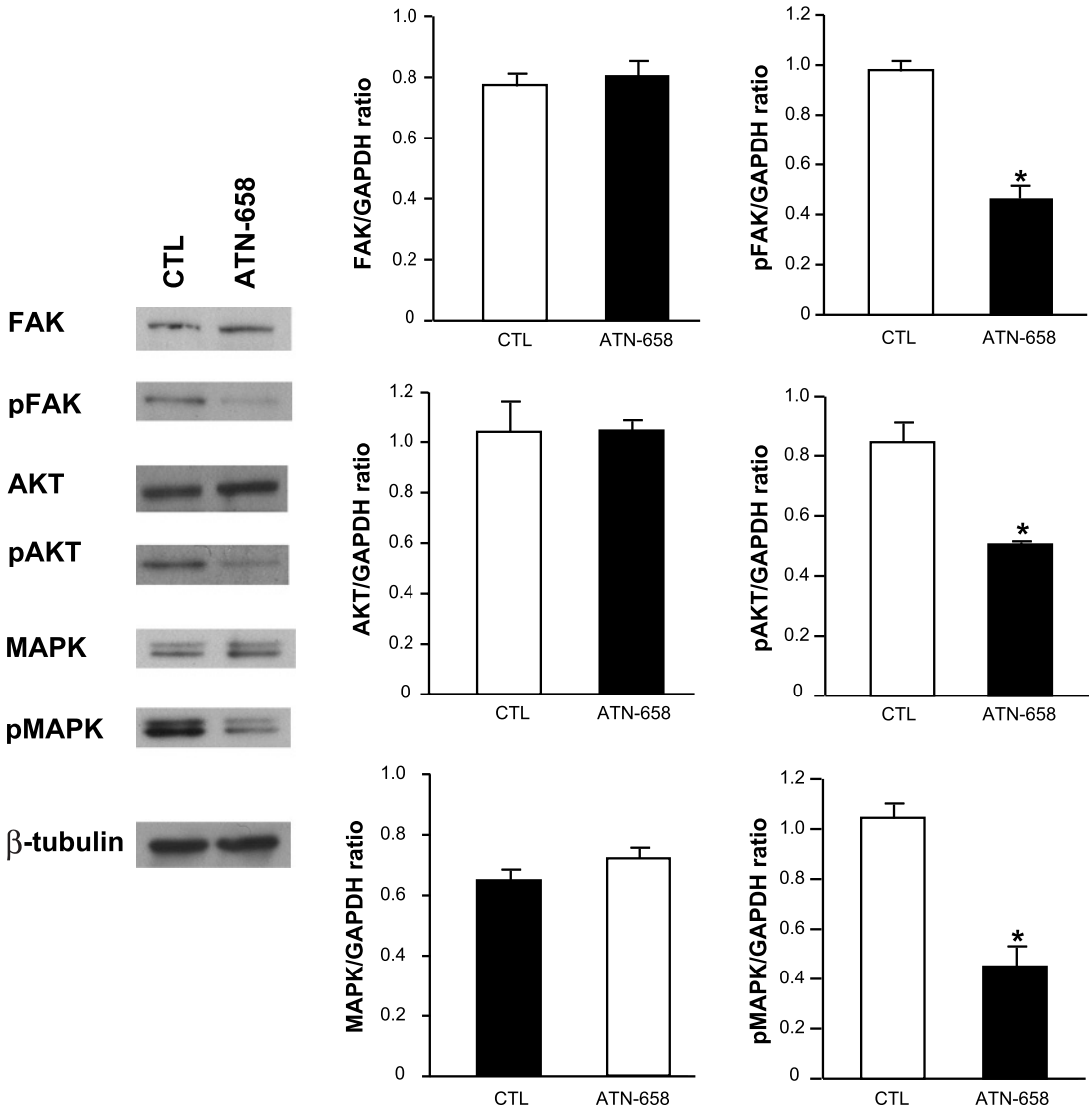

Figure 2. Inhibition of tyrosine phosphorylation of signaling intermediates by ATN-658. PC-3 cells were treated with 50.0 μg/ml of control IgG (CTL) or ATN-658 for 24 hours. Cells were harvested, and 40 μg of total cellular protein was subjected to Western blot analysis as described in Materials and Methods using antibodies against AKT, phosphorylated (p) AKT, MAPK, pMAPK, FAK, and pFAK. Anti–β-tubulin antibody was used as loading control. Levels of expression of these proteins were determined by densitometric scanning and represented as relative density. Results are presented as the mean ± SEM of two different experiments. A significant difference from the control (CTL) is represented by an asterisk ($P < .05$).

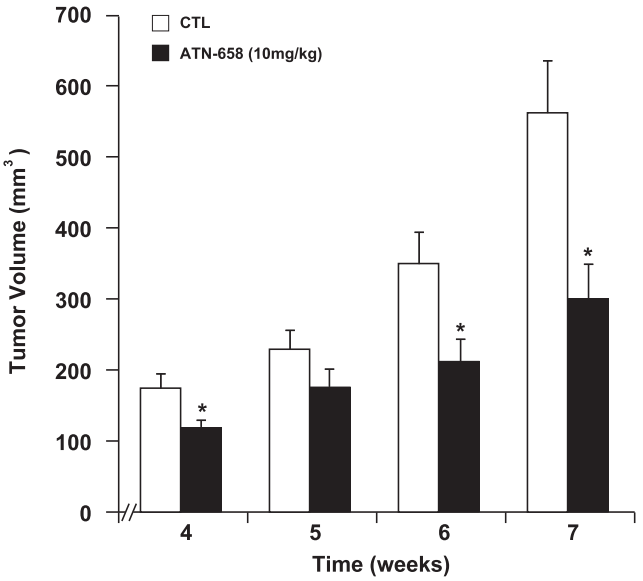

Figure 3. Effect of ATN-658 on prostate cancer growth *in vivo*. Male Balb C *nu/nu* mice were inoculated with (2×10^6) PC-3 cells through the s.c. route. Animals were treated with 10.0 mg/kg of control IgG (CTL) or ATN-658 through the i.p. route. Tumors were measured weekly, and tumor volume was determined as described in Materials and Methods. Result represents the mean ± SEM of eight animals in each group. Significant differences from control are represented by asterisks ($P < .05$).

inhibits tumor growth *in vivo* both when cells are inoculated s.c. as well as when they are inoculated i.t. in a model that we believe represents prostate cancer metastasis outgrowth in the bone. Although the inhibition of tumor growth is statistically significant when the tumors are grown s.c., the magnitude of inhibition by ATN-658 seems greater in the i.t. model. An analysis of the activation of FAK, AKT, and MAPK reveals that only MAPK activation is inhibited in the tumors grown s.c., whereas the activation of all three signaling effectors is impaired in the i.t. models. This difference in these effects on signaling may be one explanation of why ATN-658 seems to be more effective in the i.t. model. The reason for this difference between the models where the tumors are inoculated in different anatomic locations is unknown, although a simple explanation (and one hypothesis) is that the difference is due to the different pharmacology of drug delivery and tumor perfusion rather than a mechanistic explanation. For example, tumor perfusion by ATN-658 may be different when the tumor is grown s.c. compared with that in the bone (bone being highly vascularized to begin with and therefore more amenable to drug delivery of a macromolecule), and we have previously observed differences in the antitumor activity of ATN-658 depending on whether treatment was initiated when a tumor was small or large (with a greater magnitude of antitumor activity observed against larger established tumors, consistent with differences in the ability of ATN-658 to perfuse a tumor) [26]. Alternatively, the differences on signaling and tumor growth may be manifestations of differences in tumor microenvironment. For example, uPAR may engage a different set of binding partners in bone tumors compared with s.c. tumors that lead to the observed differences in the effects on signaling depending on the anatomic location of the tumor. It is well known clinically that tumors of the same so-called histologic subtype (e.g., prostate cancer) behave differently depending on the histologic location, exposure to previous treatments, and so on, and in fact, a "prostate cancer" in bone is really a different disease than prostate cancer in the prostate [27]. As an extension of these clinical observations, it is interesting to observe that in the i.t. model, ATN-658 seems to have greater efficacy with prolonged treatment. Unfortunately, it is difficult to extend this model longer than the 5-week period presented in this study to see if the increase in antitumor activity would continue because of the morbidity associated with the PC-3 lesions in the tibia of control animals once the mice pass the 5-week point. What is known is that ATN-658 does not affect the interaction of uPAR with vitronectin (VN) and does not bind to the epitope on uPAR that interacts with VN so it is unlikely that the antitumor effects of ATN-658 are mediated through altering the interaction of VN with uPAR. We have recently published the crystal structure of the VN-uPAR complex, and the epitope of ATN-658 has recently been described [28,29].

ATN-658 does not bind to mouse uPAR. In addition, although ATN-658 is a monoclonal antibody, it is an IgG1 isotype that does not mediate antibody-directed cytotoxicity in mice (this has been confirmed *in vitro* using mouse effector and tumor cells; data not shown).

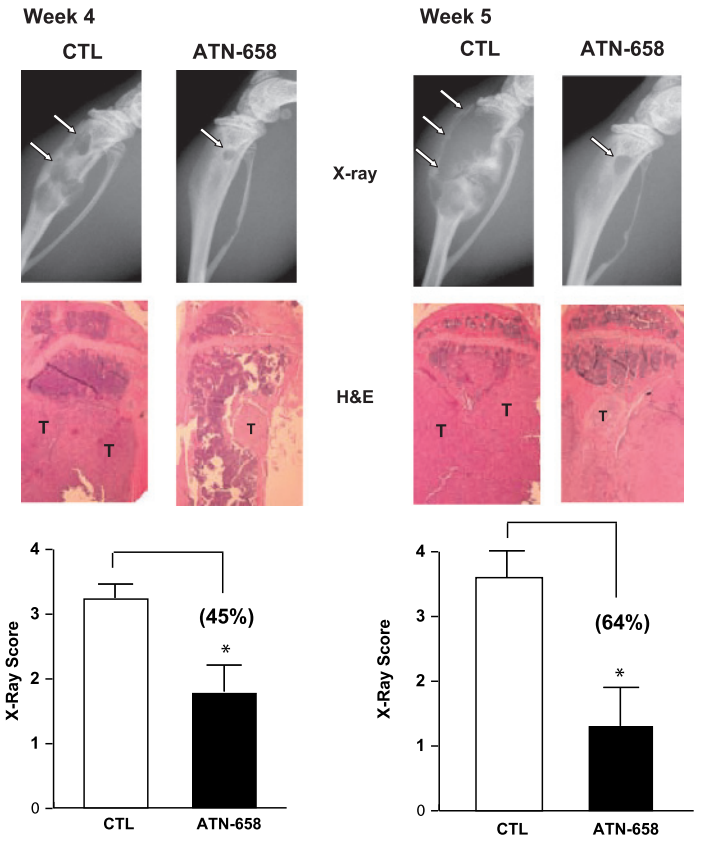

Figure 4. Effect of ATN-658 on prostate cancer skeletal lesions *in vivo*. Male Fox Chase SCID mice were inoculated with (2×10^6) PC-3 cells through the i.t. route. Animals were treated with 10.0 mg/kg of control IgG (CTL) or ATN-658 through the i.p. route. Development of skeletal lesions was determined at weekly intervals by x-ray using Faxitron, and lesion area was determined as described in Materials and Methods. Skeletal lesions in radiographs are highlighted by arrows, and histologic analysis was carried by hematoxylin and eosin (H&E) staining where i.t. tumors are marked as "T". Representative radiograph lesion score of control and experimental animals at weeks 4 and 5 after tumor cell inoculation is shown in lower panels. Result represents the mean ± SEM of eight animals in each group. Significant differences from control are represented by asterisks ($P < .05$).

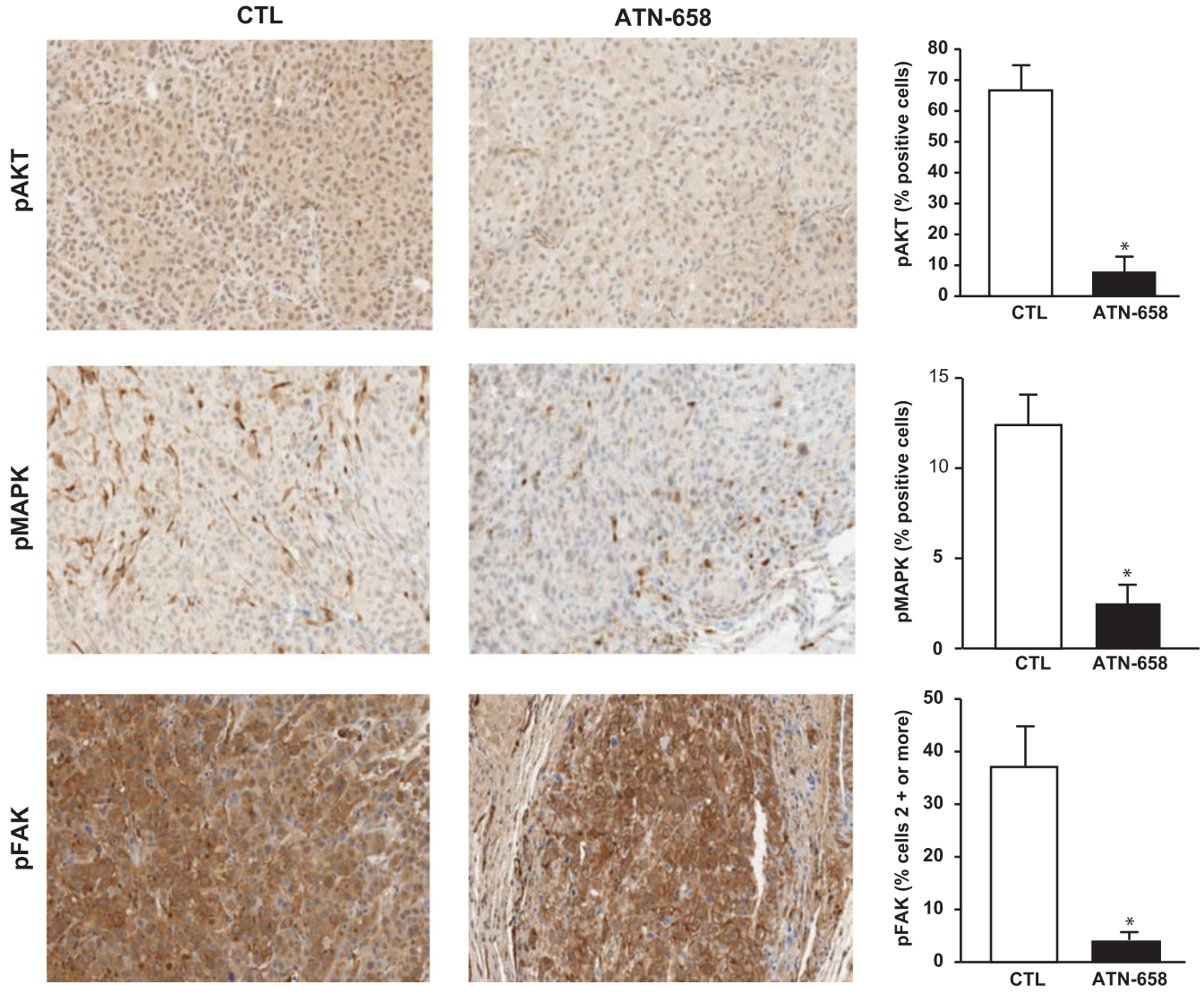

Figure 5. ATN-658 inhibits the expression of signaling molecules in prostate cancer tumors and skeletal lesions *in vivo*. Male Fox chase SCID mice were inoculated with PC-3 cells through the i.t. route of injection, respectively. Animals were treated with 10.0 mg/kg of control IgG (CTL) or ATN-658. At the end of these studies, animals were killed, and tibias were removed, formalin-fixed, and subjected to immunohistochemical analysis as described in Materials and Methods. Result represents the mean ± SEM of five tibias from each group. Significant differences from control are represented by asterisks ($P < .05$).

Thus, the antitumor effects that are observed in this study are likely due to the antagonistic effects of ATN-658 against the human uPAR expressed by the implanted PC-3 tumor cells. Using immunohistochemical analysis of i.t. tumors, no effects of ATN-658 on apoptosis were observed using CC3 as a marker. In addition and not surprisingly given the lack of ATN-658's ability to bind to host-derived uPAR, no effects were observed on angiogenesis using CD31 immunostaining (data not shown). In contrast, ATN-658 strongly inhibited tumor cell proliferation (Figure 6), consistent with a previous study evaluating ATN-658 in a model of pancreatic carcinoma, and also led to the down-regulation of uPAR expression on the tumor cells [18]. In addition, despite the fact that uPAR is expressed on PC-3 cells in culture, some of these cells lose uPAR expression when grown *in vivo* because uPAR does not seem to expressed by all cells within a PC-3 tumor even in nontreated controls (Figure 6). Thus, the apparent antitumor activity of ATN-658 may be dampened *in vivo* if the expression of uPAR is, for some reason, lost in some of the tumor cells. The loss of uPAR expression by the PC-3 cells *in vivo* is currently not understood but could be attributable to a number of reasons that contribute to tumor heterogeneity including differences in the interaction with the tumor microenvironment that might occur in different parts of the tumor and differences in tumor oxygenation. In humans, we would predict that this antibody would have the potential for even greater antitumor activity than that observed in these mouse models because in addition to tumor cells per se, the antibody would also target uPAR expressed on angiogenic endothelium and tumor-associated infiltrating cells such as neutrophils and macrophages, both of which can contribute to tumor progression [30]. In cancer patients, soluble uPAR (suPAR) may also be present and may be relevant to disease progression. For example, suPAR has been demonstrated to be associated with poor prognosis in patients with ovarian cancer [31]. One concern is that high levels of suPAR may alter the activity of ATN-658 by acting as a sink for the antibody and sequestering its availability from delivery to the tumor. As described in the Results, we are able to achieve micromolar steady-state concentrations

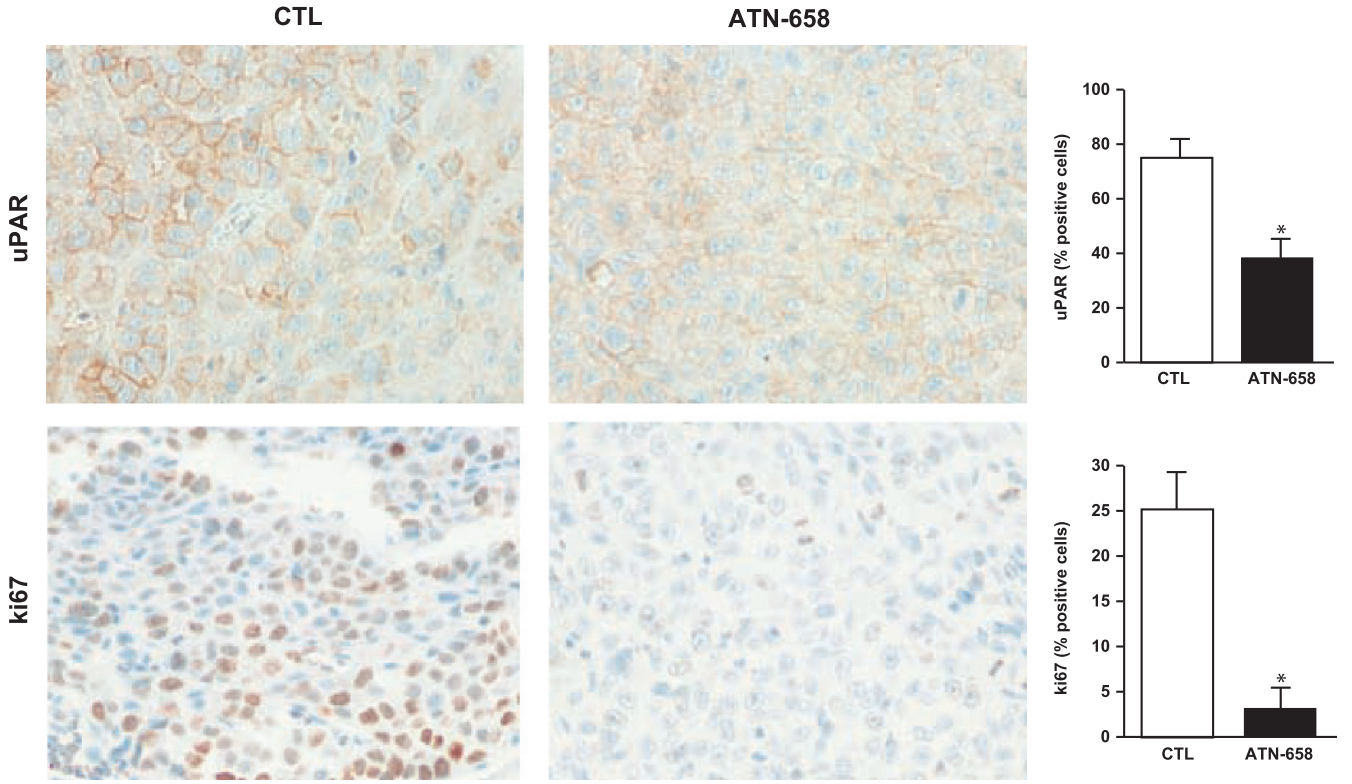

Figure 6. ATN-658 inhibits tumor cell proliferation and uPAR expression *in vivo*. Male Fox chase SCID mice were inoculated with PC-3 cells through the i.t. route of injection, respectively. Animals were treated with 10.0 mg/kg of control IgG (CTL) or ATN-658. At the end of these studies, animals were killed, and tibias were removed, formalin-fixed, and subjected to immunohistochemical analysis using antibodies against Ki67 and uPAR as described in Materials and Methods. Result represents the mean ± SEM of three tibias from each group. Significant differences from control are represented by asterisks ($P < .05$).

of ATN-658, whereas the levels of suPAR in cancer patients are on the order of nanograms per milliliter (fM). Thus, little or no effect of suPAR on ATN-658 plasma levels is predicted. ATN-658 has now been humanized and is currently in late-stage preclinical development. Despite the fact that a number of questions remain regarding the mechanism of action of how ATN-658 exerts its antitumor effects at the molecular level, there is a sufficient body of basic evidence that supports advancing the humanized version of ATN-658 into clinical evaluation. In addition, the bulk of Investigational New Drug Application–enabling studies have already been completed, and thus, the humanized version of ATN-658 (huATN-658) is expected to imminently enter a phase 1 clinical study. Thus, the hypothesis that uPAR represents a validated tumor target in human cancer and that therapeutically targeting this receptor will have clinical benefit in cancer patients will begin evaluation in the near future.

References

[1] Cozzi PJ, Wang J, Delprado W, Madigan MC, Fairy S, Russell PJ, and Li Y (2006). Evaluation of urokinase plasminogen activator and its receptor in different grades of human prostate cancer. *Hum Pathol* **37**, 1442–1451.

[2] Yamamoto M, Sawaya R, Mohanam S, Rao VH, Bruner JM, Nicolson GL, and Rao JS (1994). Expression and localization of urokinase-type plasminogen activator receptor in human gliomas. *Cancer Res* **54**, 5016–5020.

[3] Hildenbrand R and Schaaf A (2009). The urokinase-system in tumor tissue stroma of the breast and breast cancer cell invasion. *Int J Oncol* **34**, 15–23.

[4] Thomas C, Wiesner C, Melchior SW, Schmidt F, Gillitzer R, Thüroff JW, and Pfitzenmaier J (2009). Urokinase-plasminogen-activator receptor expression in disseminated tumour cells in the bone marrow and peripheral blood of patients with clinically localized prostate cancer. *BJU Int* **104**, 29–34.

[5] Gupta A, Lotan Y, Ashfaq R, Roehrborn CG, Raj GV, Aragaki CC, Montorsi F, and Shariat SF (2008). Predictive value of the differential expression of the urokinase plasminogen activation axis in radical prostatectomy patients. *Eur Urol* **55**, 1124–1133.

[6] Subramanian R, Gondi CS, Lakka SS, Jutla A, and Rao JS (2006). siRNA-mediated simultaneous downregulation of uPA and its receptor inhibits angiogenesis and invasiveness triggering apoptosis in breast cancer cells. *Int J Oncol* **28**, 831–839.

[7] Pulukuri SM, Gondi CS, Lakka SS, Jutla A, Estes N, Gujrati M, and Rao JS (2005). RNA interference–directed knockdown of urokinase plasminogen activator and urokinase plasminogen activator receptor inhibits prostate cancer cell invasion, survival, and tumorigenicity *in vivo*. *J Biol Chem* **280**, 36529–36540.

[8] Bu X, Khankaldyyan V, Gonzales-Gomez I, Groshen S, Ye W, Zhuo S, Pons J, Stratton JR, Rosenberg S, and Laug WE (2004). Species-specific urokinase receptor ligands reduce glioma growth and increase survival primarily by an antiangiogenesis mechanism. *Lab Invest* **84**, 667–678.

[9] Wilhelm O, Weidle U, Höhl S, Rettenberger P, Schmitt M, and Graeff H (1994). Recombinant soluble urokinase receptor as a scavenger for urokinase-type plasminogen activator (uPA). Inhibition of proliferation and invasion of human ovarian cancer cells. *FEBS Lett* **337**, 131–134.

[10] Ellis V, Behrendt N, and Danø K (1991). Plasminogen activation by receptor-bound urokinase. A kinetic study with both cell-associated and isolated receptor. *J Biol Chem* **266**, 12752–12758.

[11] Kobayashi H, Gotoh J, Fujie M, Shinohara H, Moniwa N, and Terao T (1994). Inhibition of metastasis of Lewis lung carcinoma by a synthetic peptide within growth factor-like domain of urokinase in the experimental and spontaneous metastasis model. *Int J Cancer* **57**, 727–733.

[12] Hu XW, Duan HF, Gao LH, Pan SY, Li YM, Xi Y, Zhao SR, Yin L, Li JF, Chen HP, et al. (2008). Inhibition of tumor growth and metastasis by ATF-Fc, an engineered antibody targeting urokinase receptor. *Cancer Biol Ther* **7**, 651–659.

[13] Tang CH, Hill ML, Brumwell AN, Chapman HA, and Wei Y (2008). Signaling through urokinase and urokinase receptor in lung cancer cells requires interactions with {beta}1 integrins. *J Cell Sci* **121**, 3747–3756.

[14] Zhang F, Tom CC, Kugler MC, Ching TT, Kreidberg JA, Wei Y, and Chapman HA (2003). Distinct ligand binding sites in integrin $\alpha_3\beta_1$ regulate matrix adhesion and cell-cell contact. *J Cell Biol* **163**, 177–188.

[15] Okumura Y, Kamikubo Y, Curriden SA, Wang J, Kiwada T, Futaki S, Kitagawa K, and Loskutoff DJ (2002). Kinetic analysis of the interaction between vitronectin and the urokinase receptor. *J Biol Chem* **277**, 9395–9404.

[16] Margheri F, D'Alessio S, Serratí S, Pucci M, Annunziato F, Cosmi L, Liotta F, Angeli R, Angelucci A, Gravina GL, et al. (2005). Effects of blocking urokinase receptor signaling by antisense oligonucleotides in a mouse model of experimental prostate cancer bone metastases. *Gene Ther* **12**, 702–714.

[17] Mohan PM, Chintala SK, Mohanam S, Gladson CL, Kim ES, Gokaslan ZA, Lakka SS, Roth JA, Fang B, Sawaya R, et al. (1999). Adenovirus-mediated delivery of antisense gene to urokinase-type plasminogen activator receptor suppresses glioma invasion and tumor growth. *Cancer Res* **59**, 3369–3373.

[18] Bauer TW, Liu W, Fan F, Camp ER, Yang A, Somcio RJ, Bucana CD, Callahan J, Parry GC, Evans DB, et al. (2005). Targeting of urokinase plasminogen activator receptor in human pancreatic carcinoma cells inhibits c-Met– and insulin-like growth factor-I receptor–mediated migration and invasion and orthotopic tumor growth in mice. *Cancer Res* **65**, 7775–7781.

[19] Bdeir K, Kuo A, Mazar A, Sachais BS, Xiao W, Gawlak S, Harris S, Higazi AA, and Cines DB (2000). A region in domain II of the urokinase receptor required for urokinase binding. *J Biol Chem* **275**, 28532–28538.

[20] Guo Y, Mazar AP, Lebrun JJ, and Rabbani SA (2002). An antiangiogenic urokinase-derived peptide combined with tamoxifen decreases tumor growth and metastasis in a syngeneic model of breast cancer. *Cancer Res* **62**, 4678–4684.

[21] Yang M, Burton DW, Geller J, Hillegonds DJ, Hastings RH, Deftos LJ, and Hoffman RM (2006). The bisphosphonate olpadronate inhibits skeletal prostate cancer progression in a green fluorescent protein nude mouse model. *Clin Cancer Res* **12**, 2602–2606.

[22] Khalili P, Arakelian A, Chen G, Plunkett ML, Beck I, Parry GC, Doñate F, Shaw DE, Mazar AP, and Rabbani SA (2006). A non–RGD-based integrin binding peptide (ATN-161) blocks breast cancer growth and metastasis *in vivo*. *Mol Cancer Ther* **9**, 2271–2280.

[23] Carriero MV, Del Vecchio S, Capozzoli M, Franco P, Fontana L, Zannetti A, Botti G, D'Aiuto G, Salvatore M, and Stoppelli MP (1999). Urokinase receptor interacts with $\alpha(v)\beta_5$ vitronectin receptor, promoting urokinase-dependent cell migration in breast cancer. *Cancer Res* **59**, 5307–5314.

[24] D'Alessio S and Blasi F (2009). The urokinase receptor as an entertainer of signal transduction. *Front Biosci* **14**, 4575–4787.

[25] Gondi CS, Kandhukuri N, Dinh DH, Gujrati M, and Rao JS (2007). Down-regulation of uPAR and uPA activates caspase-mediated apoptosis and inhibits the PI3K/AKT pathway. *Int J Oncol* **31**, 19–27.

[26] Van Buren G II, Gray MJ, Dallas NA, Xia L, Lim SJ, Fan F, Mazar AP, and Ellis LM (2009). Targeting the urokinase plasminogen activator receptor (uPAR) with a monoclonal antibody impairs the growth of human colorectal cancer in the liver. *Cancer* **115**, 3360–3368.

[27] Coleman RE (2006). Clinical features of metastatic bone disease and risk of skeletal morbidity. *Clin Cancer Res* **12**, 6243s–6249s.

[28] Huai Q, Zhou A, Lin L, Mazar AP, Parry GC, Callahan J, Shaw DE, Furie B, Furie BC, and Huang M (2008). Crystal structures of two human vitronectin, urokinase and urokinase receptor complexes. *Nat Struct Mol Biol* **15**, 422–423.

[29] Mazar AP, Ternansky RJ, Parry GC, Gladstone PL, and Gawlak S, inventors. Antibodies and/or conjugates thereof which bind to the amino terminal fragment of urokinase, compositions and uses thereof. WO/2005/048822. June 2, 2005.

[30] Alberti C (2008). Genetic and microenvironmental implications in prostate cancer progression and metastasis. *Eur Rev Med Pharmacol Sci* **12**, 167–175.

[31] Henić E, Borgfeldt C, Christensen IJ, Casslén B, and Høyer-Hansen G (2008). Cleaved forms of the urokinase plasminogen activator receptor in plasma have diagnostic potential and predict postoperative survival in patients with ovarian cancer. *Clin Cancer Res* **14**, 5785–5793.